CrossMark

Platinum–cobalt catalysts for the oxygen reduction reaction in high temperature proton exchange membrane fuel cells – Long term behavior under ex-situ and in-situ conditions

Alexander Schenk [a],[*], Christoph Grimmer [a], Markus Perchthaler [a],[b], Stephan Weinberger [a], Birgit Pichler [a], Christoph Heinzl [c], Christina Scheu [c], Franz-Andreas Mautner [d], Brigitte Bitschnau [d], Viktor Hacker [a]

[a] Institute of Chemical Engineering and Environmental Technology, Fuel Cell Systems Group, Graz University of Technology, Steyrergasse 21, Graz 8010, Austria
[b] elcomax GmbH, Bayerwaldstraße 3, Munich 81737, Germany
[c] Department of Chemistry, Ludwig-Maximilians-University Munich, Butenandtstr. 11, Munich 81377, Germany
[d] Institute of Physical and Theoretical Chemistry, Structure Science Group, Graz University of Technology, Stremayrgasse 9, Graz 8010, Austria

HIGHLIGHTS

- Platinum cobalt catalysts are synthesized by a scalable straightforward process.
- Stability increasing post-preparation treatments are developed and optimized.
- RDE experiments and HT-PEM single cell tests are conducted.
- Platinum loading is reduced without loss of performance and durability.

ARTICLE INFO

ABSTRACT

Platinum cobalt catalysts (Pt–Co) have attracted much interest as cathode catalysts for proton exchange membrane fuel cells (PEMFCs) due to their high activity toward oxygen reduction reaction (ORR). Many of the reported catalysts show outstanding performance in ex-situ experiments. However, the laborious synthesis protocols of these Pt–Co catalysts disable an efficient and economic production of membrane electrode assemblies (MEAs). We present an economic, flexible and continuous Pt-M/C catalyst preparation method as part of a large scale membrane electrode assembly manufacturing. In comparison, the as-prepared Pt–Co/C based high temperature (HT)-PEM MEA showed an equal performance to a commercially available HT-PEM MEA during 600 h of operation under constant load, although the commercial one had a significantly higher Pt loading at the cathode.

© 2014 Elsevier B.V. All rights reserved.

1. Introduction

Proton exchange membrane fuel cell (PEMFC) technology enables clean and efficient energy conversion with high energy density and is therefore considered to be a key source of power in a future society based on renewable and sustainable energy. So far, this promising technology has not yet penetrated the market to compete with conventional power sources.

Platinum offers the highest catalytic activity toward oxygen reduction reaction (ORR) of any pure metals. But nevertheless the ORR activity on Pt is too slow for an efficient operation of fuel cells.

* Corresponding author. Tel.: +43 316 873 8783; fax: +43 316 873 8782.
E-mail addresses: alexander.schenk@tugraz.at (A. Schenk), christoph.grimmer@tugraz.at (C. Grimmer), Markus.Perchthaler@elcomax.com (M. Perchthaler), stephan.weinberger@tugraz.at (S. Weinberger), birgit.pichler@tugraz.at (B. Pichler), Christoph.Heinzl@cup.uni-muenchen.de (C. Heinzl), Christina.Scheu@cup.uni-muenchen.de (C. Scheu), mautner@tugraz.at (F.-A. Mautner), bitschnau@tugraz.at (B. Bitschnau), viktor.hacker@tugraz.at (V. Hacker).

Due to kinetic limitations, at present, PEMFCs require relatively high loadings of platinum. It has been shown, that the anode loading could be reduced from 0.1 to 0.05 mg cm^{-2} [1,2]. However, at the cathode, 0.4 mg cm^{-2} are required to compensate the high overpotential losses of the ORR [1,3,4]. Considering state-of-the-art high temperature PEM fuel cell technology even higher Pt loadings are used. Recent developments led to a reduction of the Pt loading at the anode to 0.9 mg cm^{-2}, whereas the cathode still required 1.7 mg cm^{-2} [5].

Over the last two decades substantial efforts have been dedicated to find new catalyst systems for fuel cells. As the replacement of Pt by catalysts made of abundant elements, which show ORR activities close to that of Pt, faces several challenges, such as long term stability in acidic media, most of the research work focusses on improving the ORR activity of Pt in fuel cells [1,3,6–12]. By using an appropriate combination of platinum with other metals (e.g. Pd, Ru, V, Cr, Co, Ni, Cu etc.) it is possible to increase the activity toward ORR significantly and hence reduce the Pt loading at the cathode [1,3,13–23]. In particular the formation of platinum alloys with late transition metals such as Co has been investigated extensively [17,21–29]. The reported Pt–Co catalysts show an increased activity toward ORR compared to pure Pt. Whereby this enhancement of the electrocatalytic ORR activity of these catalysts is related to the weaker binding of the surface to ORR intermediates, e.g. HO* [1,3,4,14–17,23].

Although these Pt-M catalysts offer several advantages for PEMFC technology, there are further improvements to be achieved. Especially the highly corrosive conditions in PEM fuel cells result in gradual dissolution of the transition metal, the agglomeration of platinum or its loss to the electrolyte and consequently to a loss of power density [1,3,29–33]. Hence, the combination of advanced catalyst development, functionalization of support materials, appropriate membrane manufacturing and the methods of their composition lay the foundation for a large-scale catalyst and membrane electrode assembly production and is the crucial step toward commercialization of fuel cell technology.

In literature many approaches and methods can be found for the synthesis of carbon supported platinum alloy nanoparticles Pt-M/C. In order to keep an easily up-scalable production process in mind, it is most likely to use solution-based chemical approaches, such as impregnation. For impregnation metal precursor salts are dissolved in an appropriate solvent and then merged with a suitable support material, usually high surface area carbon (HSAC). The precursor solution wets the pores of the support material by capillary forces. The product is dried afterwards to remove excess solvent, heated and finally reduced to give the corresponding metals. In order to increase the reaction rate and to directly convert the metal salts into metallic nanoparticles a reducing agent, e.g. ethylene glycol, is added to the impregnation solution. Additionally, the as-prepared catalysts can be leached in acid solution to remove the inactive transition metal from the catalysts surface, leading to a so-called Pt-skeleton surface [1,14,28,33]. A heat treatment of the Pt-M/C catalysts, depending on the temperature, can either be used to decompose any undesired organic residues or to rearrange the positioning of Pt and M within the catalysts [28,34]. Due to the lower surface energy of Pt, in comparison to the transition metal in inert atmosphere, platinum migrates to the catalysts surface, leading to a so-called Pt-skin structure [1,14,28,33]. Both processes, leaching and heat treatment, form a Pt overlayer at the surface of the Pt-M catalysts and induce through strain and ligand effects a weakening of the binding of ORR intermediates at the Pt surface, hence leading to a higher activity toward ORR [1,33]. Furthermore, the Pt overlayer renders the Pt-M catalysts kinetically stable against dissolution of the solute transition metal under the acidic and oxidizing environment of the (HT-)PEM fuel cell cathode [1,33].

In this paper we present an economic, flexible and continuous Pt-M/C catalyst preparation as part of a large scale MEA manufacturing. The given MEA manufacturing process consists of the following production steps: (i) deposition of high surface area carbon (HSAC) on carbon paper, (ii) impregnation with metal salt containing solutions, (iii) reduction of the precursor salts, (iv) stabilization of the Pt-M catalysts, (v) doping with phosphoric acid and (vi) assembling of the MEA.

The focus of our work was set on the establishment of an active and stable catalyst system, which opens up the possibility for the reduction of the precious metal loading, thus a cost reduction of a state-of-the-art membrane electrode assembly. Every single step of the MEA manufacturing has been designed to fit into a continuous production process, such as roll-to-roll production. The continuous deposition of the catalysts directly in the, for HT PEM usage optimized, porous layer of the gas diffusion electrode leads to a better utilization of Pt. In contrast, conventional impregnation of catalysts onto HSAC and casting it afterwards onto the gas diffusion layer leads to a higher loss of Pt during the production and therefore to a more expensive process. Furthermore, Pt can be enclosed in carbon aggregates during conventional deposition and is therefore lost for the electrocatalytic reactions. The herein presented continuous MEA fabrication is much more time and cost saving, since batch processes, such as conventional loading of the HSAC, filtering or centrifugation, multiple washing, drying and annealing steps in tube furnaces, are eliminated. Moreover, the scrap, which could be produced during the manufacturing of the porous layer, has no expensive catalyst in it. So, higher scrap rates can be accepted.

2. Experimental

2.1. Preparation of gas diffusion electrodes

The catalyst support (turbostratic (t-carbon or disordered graphite) HSAC, BET: 250–300 m^2 g^{-1}) material with PTFE as hydrophobic binder material was applied on a wet proofed carbon based gas diffusion layer via a doctor blade process. The catalyst support slurry consists of the HSAC, a PTFE dispersion (Dyneon™, TF 5035 PTFE), deionized water and 2-propanol (gradient grade, Merck). The gap of the doctor blade was adjusted to 610 μm to get an optimal loading of carbon/PTFE on the gas diffusion layer. The prepared gas diffusion electrode (GDE) was dried at 170 °C under constant air flow.

2.2. Catalyst preparation

All chemicals were used as purchased without further purification.

An optimized deposition of the nanocrystalline platinum cobalt catalysts supported on HSAC (Pt–Co/C) was obtained by adjusting the composition of the precursor solution, the reducing atmosphere, the temperature and the atomic ratio of platinum and cobalt salts as a function of each other, respectively. The impregnation solution was drop-coated on previously fabricated GDE sheets, resulting in a platinum loading of 1.00 mg cm^{-2}. In order to achieve a cheap and easy deposition of the catalysts, we obtained best results with an impregnation solution, having a Pt:Co ratio of 1:5. The solution contained hexachloroplatinic acid (H$_2$PtCl$_6$*6H$_2$O, Sigma–Aldrich), cobalt nitrate (Co(NO$_3$)$_2$*6H$_2$O, Sigma–Aldrich), ethylene glycol (EG, Carl Roth) as reducing agent and 2-propanol (Sigma–Aldrich)/ultrapure water (18.1 MΩ cm, Barnstead nanopure) (1:1) as solvent. Furthermore, activity and stability enhancing treatment of the active catalyst layer includes the addition of a non-ionic surfactant (Brij-30, Sigma–Aldrich) to the precursor solution to prevent the nanoparticles from agglomeration during the reduction

step, acid leaching and annealing steps after reduction [35]. The reduction of the deposited metal salts was initiated by a mild thermal treatment at 240 °C in nitrogen atmosphere. Conducted post-preparation treatments of Pt:Co 1:5 catalysts and their combinations are given in Table 1.

A commercially available Pt/C catalyst sample was obtained from elcomax GmbH and used as reference.

2.3. MEA preparation

After the deposition of the cathode catalysts on the GDE as described above, the HT-PEM MEAs were manufactured by doping the catalyst layer with a mixture of phosphoric acid (85 wt.%) and 1-pentanol. After evaporation of 1-pentanol at 230 °C, the electrodes were hot pressed with a membrane based on poly-benzimidazole (PBI) at 150 °C to form the membrane electrode assembly.

The membranes were casted from a solution based on PBI and dimethylacetamide (N,N-DMAc, synthesis grade, Merck). Therefor meta-PBI powder was dissolved in DMAc under stirring for 3 h at 200 °C under pressure. All chemicals were used as purchased without further purification. The membranes were casted by solvent evaporation at 70–100 °C on a carrier foil. Afterwards, a thermal treatment of the membranes, to remove DMAc residues, was performed.

For the anode a standard Pt based GDE from elcomax GmbH was used. The reference HT-PEM MEA was also obtained from elcomax GmbH.

2.4. Structural and chemical analysis

A FEI Titan 80 − 300 scanning transmission electron microscope (STEM) equipped with an EDAX energy dispersive X-ray spectroscopy (EDX) detector for analytical measurements was used for the investigation of the catalysts nanoparticles. The measurements were performed at 300 kV. The electrode material was suspended in 2-propanol/water (1:1), ultrasonicated for 10 min and one droplet of the suspension was dripped on a holey carbon coated nickel grid. The crystal structure was determined via electron diffraction patterns measured over several nanoparticles and by analyzing high resolution TEM micrographs. In addition, the size and distribution of the catalyst particles was determined by TEM.

X-ray powder diffraction profiles were obtained on a Bruker AXS D8 Advance powder diffractometer in Bragg-Brentano θ-θ geometry operated at 40 kV and 40 mA, using Cu K$_\alpha$ radiation (λ = 1.54178 Å). The 2θ diffraction angles were measured by scanning the goniometer from 30 to 138° 2θ having a step size of 0.025° 2θ. The profile-fit was performed using PANalytical X'Pert High Score Plus software using the crystal structure data of metallic Pt [36] and Co [37]. Calculations using Vegard's law [38] support the observed shifts in the peaks when compared to those for pure Pt and Co. The average primary crystallite sizes of the samples (d_{xRD}) were determined according to the broadening of the diffraction peaks using the Scherrer relationship [39]

$(d_{xRD}=(K\lambda)/\Delta(2\theta)\cos\theta)$ where d is the mean crystallite dimension, K is the shape factor (0.9), λ is the X-ray wavelength in nm, $\Delta(2\theta)$ is the peak broadening at full width at half-maximum in radians and θ is the Bragg angle.

2.5. Electrochemical studies

Electrochemical studies were conducted in 0.1 M HClO$_4$ as electrolyte at room temperature and in a 50 cm^2 HT-PEMFC single cell at 160 °C, respectively. Ex-situ characterization served for preliminary evaluation and screening of the catalysts; whereas, in-situ studies were carried out using the most auspicious formulation.

2.5.1. Ex-situ characterization

All glassware was cleaned for 24 h in sulfuric acid solution, followed by heating and rinsing with ultrapure water to remove sulfate residues. The electrochemical experiments were carried out using an Autolab PGSTAT302N potentiostat (Metrohm Autolab B.V.), controlled by a computer. The rotating disc electrode (RDE) assembly was a combination of a rotator and an electrode from Pine Instruments Company (AFE5T050GC). Prior to electrode preparation, the glassy carbon rotating electrode disc was polished to a mirror finish using a 0.05 μm alumina suspension (MasterPrep, Buehler).

The electrolyte, 0.1 M HClO$_4$ (Fixanal, Fluka Analytical), was prepared with ultrapure water. The working electrode was a commercial glassy carbon disc electrode of 5 mm fixed diameter. A platinized titanium rod (Bank Elektronik − Intelligent Controls GmbH) was used as counter electrode and the reference electrode was a reversible hydrogen electrode (RHE, Hydroflex, Gaskatel Gesellschaft für Gassysteme durch Katalyse und Elektrochemie mbH). Hence, all potentials reported here are quoted with respect to RHE and are corrected for ohmic losses. 0 V$_{RHE}$ was controlled subsequently after each measurement by performing the hydrogen evolution reaction on Pt in the same electrolyte. The internal resistance drop was determined by carrying out an impedance spectrum with a peak-to-peak amplitude of 10 mV in the range from 100 kHz to 1 Hz. The ohmic drop was evaluated from the high frequency intercept point on the real axis of the Nyquist plot. Typically the uncompensated resistance came to 25–30 Ω. RDE measurements were conducted in a nitrogen (5.0, Messer Group GmbH) saturated electrolyte, whereas, the oxygen reduction reaction (ORR) activity measurements were performed in an electrolyte saturated with oxygen (5.5, Messer Group GmbH). During measurement the oxygen supply was sustained to keep the oxygen concentration in solution at a constant level.

In order to prepare the rotating disc electrodes for cyclic voltammetry and ORR measurements, 2 cm^2 of the impregnated gas diffusion electrodes were suspended in 2-propanol and treated in an ultrasonic bath to form a homogeneous catalysts dispersion. A 10 μl aliquot of the dispersion was dispensed onto the working electrode resulting in a loading of 28 μg$_{Pt}$ cm^{-2} geometric surface area.

The electrocatalysts were pre-treated using 250 cyclic voltammetry scans between 0.050 and 1.255 V$_{RHE}$ at a scan rate of 500 mV s^{-1}. Afterwards, an analysis cycle was performed from 0.050 to 1.055 V$_{RHE}$ at 50 mV s^{-1}. The electrochemical active platinum surface area (ECSA) was determined from the mean integral charge Q of the hydrogen adsorption/desorption area (H$_{upd}$) after double-layer correction, considering 210 μC cm$_{Pt}^{-2}$ as conversion factor [3,40] according to Eq. (1). L$_{Pt}$ is the Pt loading on the working electrode (mg$_{Pt}$ cm^{-2}) and A$_g$ (cm^2) is the geometric surface of the glassy carbon electrode and the cathode for HT-PEM in-situ ECSA determination, respectively.

Table 1
Nomenclature of the prepared Pt–Co/C catalysts and their post-preparation treatments.

Pt–Co/C	1st Treatment	2nd Treatment
untreated	–	–
leached	Leaching, 10 vol.% H$_2$SO$_4$	–
leached + HT	Leaching, 10 vol.% H$_2$SO$_4$	Ramped annealing, starting at 30 °C, 5 °C min^{-1} to 220 °C, dwell 45 min

$$\mathrm{ECSA}\left(\mathrm{cm}^2 \ \mathrm{mg_{Pt}^{-1}}\right) = \frac{Q_{\mathrm{Hupd}}(C)}{210 \times 10^{-6} \ \mathrm{C} \ \mathrm{cm_{Pt}^{-2}} L_{\mathrm{Pt}}\left(\mathrm{mg_{Pt}} \ \mathrm{cm^{-2}}\right) A_g\left(\mathrm{cm}^2\right)} \tag{1}$$

To investigate the ORR activity potential sweeps between 0.050 and 1.055 V with a scan rate of 50 mV s^{-1} were conducted at a rotating speed of 1600 rpm. The specific current density (specific activity, SA) and the mass activity (MA) were calculated at 0.9 V$_{\mathrm{RHE}}$, respectively [41].

In order to determine the stability and durability of the as-prepared catalyst samples accelerated stress tests (AST) were conducted. Therefore, the electrodes were cycled 1665 times between 0.5 and 1.4 V$_{\mathrm{RHE}}$ in deaerated 0.1 M HClO$_4$ at a scan rate of 500 mV s^{-1}. Every 555th cycle the ECSA was determined. The loss of ECSA gives information on the stability of the synthesized Pt–Co electrocatalysts.

2.5.2. In-situ characterization

2.5.2.1. Polarization curves.
A single cell setup with an active area of 50 cm^2 and a serpentine channel flow field structure on anode and cathode was chosen. Reactant flow rates were measured and controlled using mass flow controllers. Cell temperature was set to 160 °C controlled by electrical heating cartridges and the stoichiometries were kept constant at 1.2 for hydrogen (3.0, Westfalen AG) or synthetic reformate (76.0% H$_2$, 1.2% CO and 22.8% CO$_2$, Westfalen AG) and 2.0 for air, respectively.

2.5.2.2. Long term operation under constant load.
Long term operation under constant load was conducted at a current density of 0.2 A cm^{-2} and at a temperature of 160 °C. The single cell was fueled with hydrogen on the anode with a stoichiometry of 1.2 and air at the cathode with a stoichiometry of 2.0.

2.5.2.3. Cyclic voltammetry.
Cyclic voltammograms were recorded using a Zahner power potentiostat (PP241, Zahner Elektrik) and a Zahner electrochemical workstation (IM6ex, Zahner Elektrik). The MEAs were tested in a 50 cm^2 single cell and fed with dry hydrogen on the anode (which was also used as pseudo-reference electrode) and humidified nitrogen on the cathode. The ECSA was determined by cycling the cathode between 0.095 and 1.100 V with 100 mV s^{-1} 100 times, followed by an analysis scan with 50 mV s^{-1}. The ECSA was calculated according to Eq. (1).

#### 2.5.2.4. Electrochemical impedance spectroscopy.
Electrochemical impedance spectra (EIS) were recorded in a pseudo-galvanostatic mode with a Zahner power potentiostat (PP241, Zahner Elektrik) and the results are presented in Nyquist plots. The peak-to-peak amplitude was set to 5 mV at 0.2 A cm^{-2}. At the anode synthetic reformate was supplied.

Equivalent circuit (EC) analysis was used to quantify the different losses occurring in the as-prepared HT-PEM MEA.

3. Results and discussion

3.1. Structural and chemical analysis

In order to obtain information about the size of the catalysts particles as well as their distribution on the carbon electrode TEM measurements were performed. The high-resolution TEM images in Fig. 1 show the crystalline catalysts particles on the turbostratic carbon electrode before leaching and heat treatment (a) and afterwards (b). The separate spherical nanoparticles are randomly distributed across the HSAC and possess a size of 4.6 ± 1.1 nm with a minimum value of about 2.2 nm and a maximum of 7.3 nm in diameter before leaching. The average size of the nanoparticles after the leaching is 4.5 ± 0.9 nm with a minimum value of about 2.4 nm and a maximum of 7.0 nm in diameter. The morphology as well as the size of the catalysts nanoparticles did not change significantly during leaching and heat treatment. The electron diffraction patterns shown in the insets of Fig. 1 reveal the quasi polycrystallinity. The diffraction rings were obtained by averaging over several randomly oriented platinum crystals. When comparing the measured d-values with literature values for cubic platinum [42] a maximum deviation of 1.3% can be detected after leaching. Neither for cubic nor for hexagonal crystalline cobalt diffraction intensities were observed. Nevertheless, the presence of cobalt was verified via EDX measurements taken over an area of several hundred nanometers in dimension. The ratio of cobalt to platinum after leaching shows that the amount of platinum with 96.5 ± 1.3 at.% highly outweighs the contained amount of cobalt with 3.5 ± 1.3 at.%. The analysis of the elemental distribution within an individual nanoparticle was not successful due to the weak signal. Given this small quantity of cobalt, a supposed alloy of platinum and cobalt would result in only slightly modified lattice plane distances. Therefore the detection of such an alloy cannot be achieved via electron diffraction or high-resolution TEM regarding
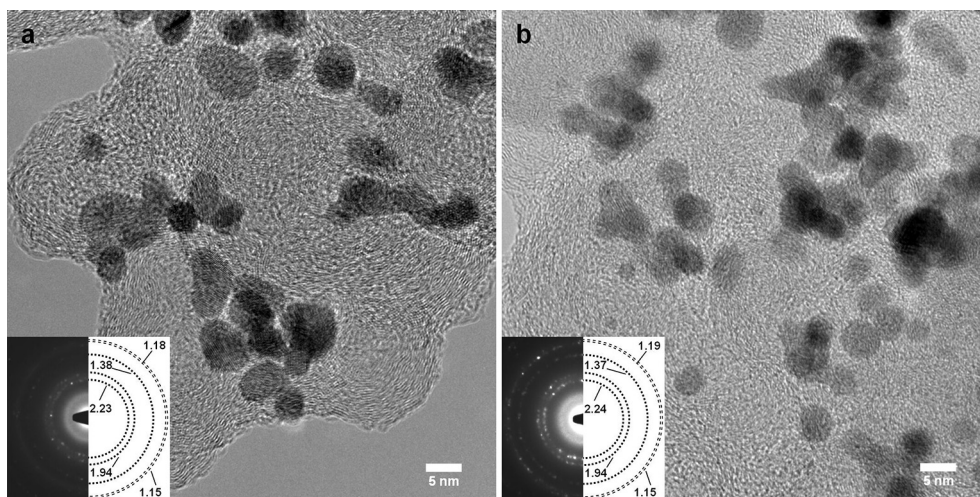
Fig. 1. High-Resolution TEM images of Pt–Co loaded HSAC before leaching and heat treatment (a) and afterwards (b). The insets show the electron diffraction patterns of the crystalline catalysts particles. The indicated d-values are given in Å.

the experimental error. EDX measurements before leaching show a significant higher ratio of cobalt (28.0 ± 6.0 at.%) to platinum (72.0 ± 6.0 at.%). Electron diffraction experiments before leaching also show intensities originating from crystalline cubic platinum only. The deviation from literature d-values (1.5%) for platinum is in the same range as for the leached sample and represents the measuring error. This finding and the fact that about 88% of the initial amount of cobalt is removed during the leaching process, lead to the assumption that most of the cobalt on the electrode was present in amorphous state.

The Pt–Co/C catalysts were further analyzed using X-ray diffraction technique. The XRD patterns of the untreated, the leached and the leached and heat treated Pt–Co/C samples as well as the Pt/C reference are given in Fig. 2. The 2θ Bragg peaks at ca. 39.8°, 46.3°, 67.7°, 81.4°, 85.5°, 103.6°, 118.1° and 123.2° correspond to the face-centered cubic (fcc) reflections of Pt(111), Pt(200), Pt(220), Pt(311), Pt(222), Pt(400), Pt(331) and Pt(420), respectively [36]. The average particle size of the catalysts was determined by using the Scherrer relationship [39]. The obtained crystallite sizes of the Pt–Co/C catalysts are within a range of 2.6–2.9 nm, whereas the particle size of the Pt/C sample is 4.1 nm. As XRD only provides the average size of the diffracting crystals rather than the particle size, the calculated crystallite sizes of the as-prepared Pt–Co/C catalysts are smaller than those determined from HR-TEM images. The Co contents within the Pt–Co/C samples were calculated by comparing the lattice parameters (a) obtained from the measured 2θ Bragg peaks with those of the commercial Pt/C catalyst ($a = 0.39147(7)$ nm), metallic Pt ($a = 0.39231$ nm) [36] and metallic Co ($a = 0.35441$ nm), respectively [37]. The lattice parameter of the commercial Pt/C sample is comparable with the previously published value of 0.39158 nm [38]. The lattice parameters of the nanocrystalline samples, the contents of Co in the Pt–Co/C catalysts derived from Vegard's law [38,43] and crystallite sizes are given in Table 2. The amounts (at.%) of Co refer to the lattice parameter of the Pt/C sample of 0.39147(7) nm. However, if the lattice parameter of metallic Pt of 0.39231 nm [36] is used as reference for Vegard's law, the Co content of the PtCo solid solutions is increased by 2.3 at.%. In both cases, the results obtained from the XRD measurements are in accordance to the EDX analysis.

3.2. Catalytic activity and degradation tests

After having discussed the structural and chemical properties of the prepared catalysts, we focus on their electrochemical and catalytic characteristics. Figs. 3 and 4 depict the beneficial effects of
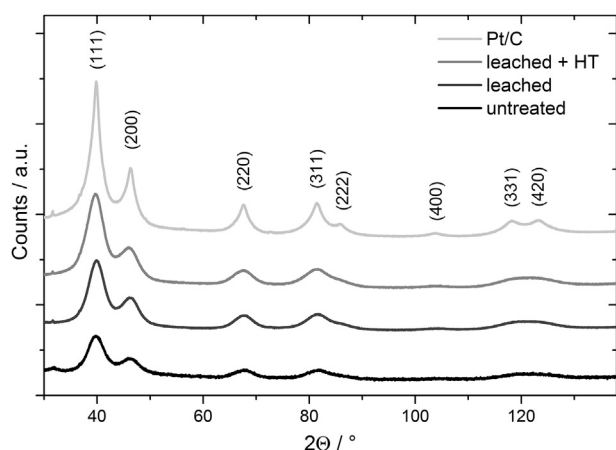
Table 2
Summary of the properties of the differently treated Pt–Co/C catalysts and the commercial Pt/C catalyst obtained from XRD measurements. The amounts (at.%) of Co refer to lattice parameter of the Pt/C sample of 0.39147(7) nm.

	a/nm	at.% Co	Size/nm
Pt–Co/C untreated	0.39013(8)	3.6	2.9
Pt–Co/C leached	0.39079(8)	1.8	2.6
Pt–Co/C leached + HT	0.39060(7)	2.4	2.6
Pt/C	0.39147(7)	–	4.1

the performed post-preparation treatments on the catalytic properties of the Pt–Co/C catalyst, which are summarized in Table 3. Fig. 4(b) shows the ORR polarization curves of the leached and heat treated Pt–Co/C catalyst and the Pt/C catalyst. Clearly, the leached and heat treated Pt–Co/C catalyst shows a more positive onset potential than the Pt/C catalyst and a higher current in the mixed-kinetic-diffusion region. The positive effect of acid-leaching on the performance of the Pt-transition metal catalysts in comparison to the Pt/C catalyst is ascribed to the dissolution of the inactive transition metal components and the segregation of Pt at the surface of the catalysts, resulting in a roughening of the surface and leaving behind a Pt-skeleton structure with a negligible amount of the solute metal [1,14,28,33]. Treating the carbon supported Pt–Co catalysts in 10 vol.% H_2SO_4 for 30 min led to a 1.7-fold increase of the specific activity (SA) and a 1.6-fold increase of the mass activity (MA) in comparison to the Pt/C sample. Additionally, a heat treatment was performed. In contrast to previously reported annealing steps in inert, reducing atmosphere or in vacuum at temperatures above 450 °C [1,28,33,44], a mild heat treatment at 220 °C in nitrogen atmosphere was performed [34,45]. The heat treatment step was initiated with an applied temperature ramp of 5 °C min^{-1} starting at 30 °C. The final temperature of 220 °C was held for 45 min; afterwards the catalyst samples were removed from the oven and cooled down to room temperature immediately. The additional heating induced a further increase of the MA of the catalysts toward ORR in comparison to the leached samples, resulting in a 2-fold activity increase over the Pt/C catalyst, whereas, the SA was not affected. The Tafel plot in Fig. 4(a) compares the electrocatalytic ORR activities of the differently treated catalysts samples to the commercial Pt/C sample.

The cyclic voltammograms (CVs) in Fig. 3, recorded in nitrogen saturated 0.1 M $HClO_4$ solution, show the typical features of Pt-based catalysts including a H_{upd} region, a double layer and an oxide formation region. The H_{upd} region reflects the catalysts

Fig. 2. X-ray diffraction patterns of the untreated, leached, the leached and heat treated Pt–Co/C catalysts and the Pt/C catalysts.
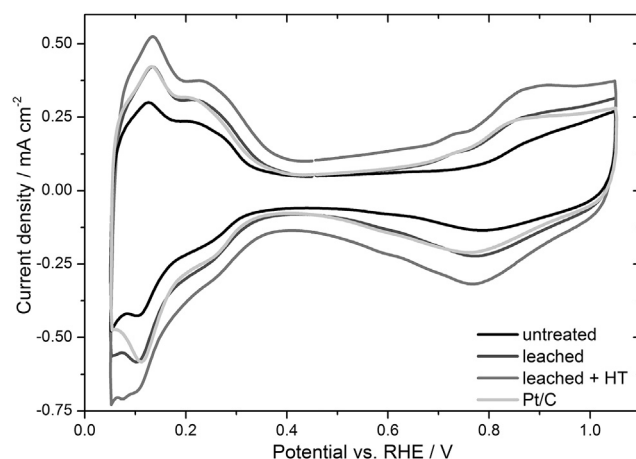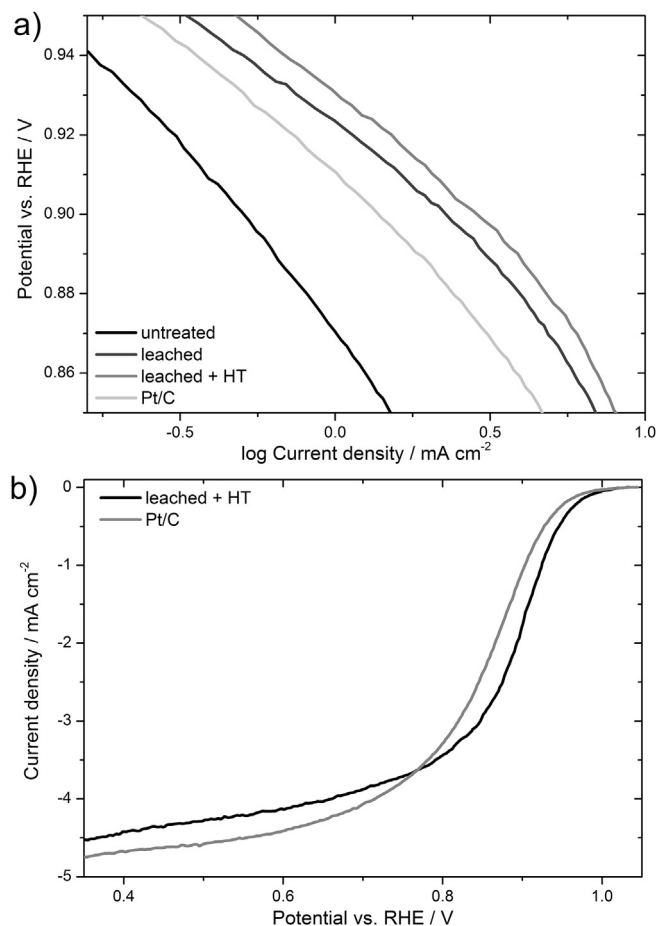

Fig. 3. Cyclic voltammograms of the as-prepared Pt–Co/C catalysts and the Pt/C reference recorded at a scan rate of 50 mV s^{-1} in nitrogen saturated 0.1 M $HClO_4$ electrolyte.

Fig. 4. (a) Tafel plots obtained from corresponding ORR polarization curves of the Pt/C and the Pt–Co/C catalyst samples, recorded at a scan rate of 50 mV s^{-1} in oxygen saturated 0.1 M HClO$_4$ electrolyte with a rotation speed of 1600 rpm. (b) Comparison of the ORR polarization curves of the leached and heat treated Pt–Co/C catalyst and the Pt/C catalyst.

electrochemical active surface area. It is evident that the catalysts reveal a higher ECSA after post-preparation treatment. As discussed above, the increase in ECSA is mainly due to the dissolution of the electrocatalytically inactive Co at the catalysts surface. Furthermore, the leaching and especially the heat treatment of the Pt–Co/C catalysts led to the removal of ethylene glycol, its decomposition products and the non-ionic surfactant from the catalysts surface. One would anticipate a decrease of ECSA during heat treatment, but using rather low temperatures, the cleaning of the catalysts surface from organic residues has a higher impact on the active surface than the increase of the mean particle size (see Fig. 3) [34,45]. However, since the annealing step is part of a continuous process, oxygen impurities in the N$_2$ atmosphere are almost unavoidable.

Table 3
Summary of the properties of the differently treated Pt–Co/C catalysts and the Pt/C reference catalyst.

	SA/ mA cm^{-2}	MA/A mg$_{Pt}^{-1}$	Roughness factor/ cm$^2_{Pt}$ cm$^{-2}_{geo}$	Initial ECSA/ cm^2 mg$_{Pt}^{-1}$	ECSA loss after 3rd AST/%
Pt–Co/C untreated	0.090	0.018	5.54	198	38
Pt–Co/C leached	0.318	0.081	7.18	257	23
Pt–Co/C leached + HT	0.322	0.100	8.68	310	20
Pt/C	0.188	0.049	7.29	260	49

Thus, the CV of the leached and heat treated catalyst exhibits an increased double layer capacitance compared to the other catalyst samples due to partial surface oxidation of the HSAC. The CV of the Pt/C catalyst sample equals the leached Pt–Co/C catalyst.

As mentioned before, due to the highly acidic and oxidizing environment of an HT-PEMFC cathode, Pt-M catalysts are prone to gradual degradation, which limits the lifetime of the PEMFC significantly. Especially high potentials (>1.2 V) lead to the corrosion of the carbon support material, the detachment of the Pt nanoparticles, their agglomeration and/or loss of electrical contact [1]. In order to determine the stability and durability of the prepared Pt–Co/C catalysts samples accelerated stress tests were conducted. Fig. 5 compares the degradation behavior of the untreated (a) to the leached and heat treated catalyst (b) and to the Pt/C reference (c). By treating the as-prepared catalysts according to the procedures mentioned above the initial ECSA as well as the stability are increased significantly. In accordance to the results obtained from XRD and TEM analysis and since the ECSA increases after leaching and heat treatment, the increase of stability cannot be attributed to an enlargement of the average particle size. We support the speculation of *Stephens* et al. that the annealing procedure smooths out the surface of the catalysts and/or removes defects of undercoordinated sites, which are most susceptible to corrosion [1].

3.3. HT-PEMFC studies

To enhance the knowledge of the interactions of the as-prepared leached and heat treated Pt–Co/C catalyst with other components inside an HT-PEM MEA, e.g. phosphoric acid, single cell tests were carried out. Furthermore, the operation in fuel cells should give information on the performance of the synthesized nanoparticles and their long term stability toward corrosion and/or de-alloying.

3.3.1. Polarization and power density

After manufacturing, the MEA was characterized by investigation of polarization, power density and electrochemical impedance properties, using hydrogen and synthetic reformate as anode feedstock, respectively. In Fig. 6 the polarization of the leached and heat treated Pt–Co/C based MEA and the commercial Pt/C based HT-PEM MEA are shown. The first polarization curve of the leached and heat treated Pt–Co/C based MEA was recorded immediately after the MEA hot pressing step; the second was taken after 600 h long term operation under a constant load of 0.2 A cm^{-1} at 160 °C. In both cases, applying pure hydrogen and synthetic reformate at the anode, the performance of the in-house prepared HT-PEM MEA was enhanced during operation. The open cell voltage (OCV) value as well as the ohmic resistance improved during the long term test. The polarization and power density of the commercial Pt/C MEA showed no change during the 600 h long term operation. While fed with hydrogen, the in-house prepared Pt–Co/C based HT-PEM MEA, having a lower Pt loading at the cathode, shows an enhanced performance over the commercial MEA after 600 h of operation, especially at higher current densities (Fig. 6(a)). However, when fueled with synthetic reformate, both MEAs exhibit an equal performance (Fig. 6(b)). The results of the durability test confirm the higher activity of the as-prepared leached and heat treated Pt–Co/C catalyst compared to the commercial Pt/C catalyst, as observed in ex-situ analysis, due to the equal performance while having less Pt.
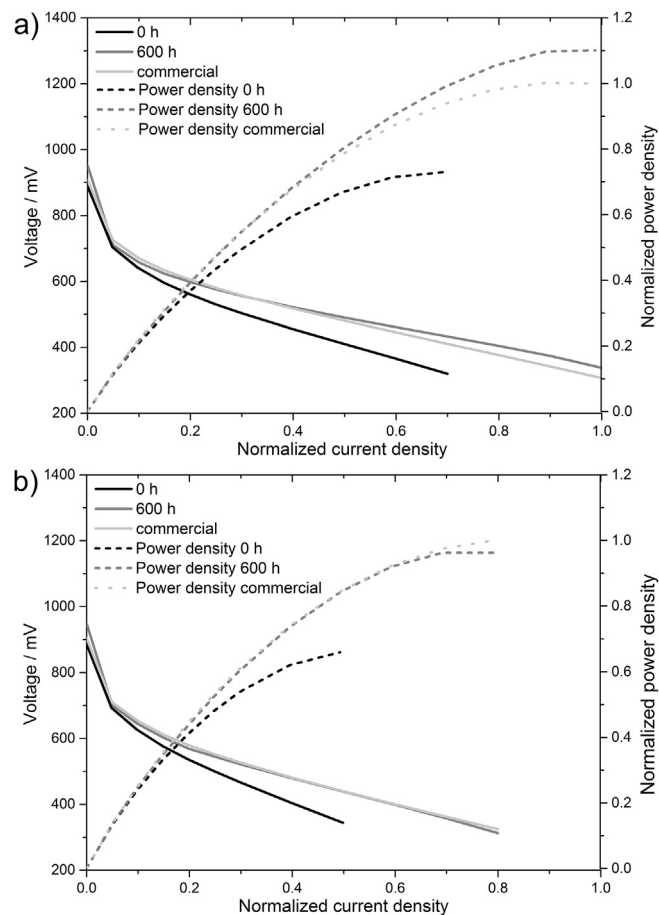
3.3.2. Long term operation under constant load

The as-prepared MEA demonstrated a good durability in single cell operation (Fig. 7). The average degradation rate of the leached and heat treated Pt–Co/C based HT-PEM MEA during the 600 h test
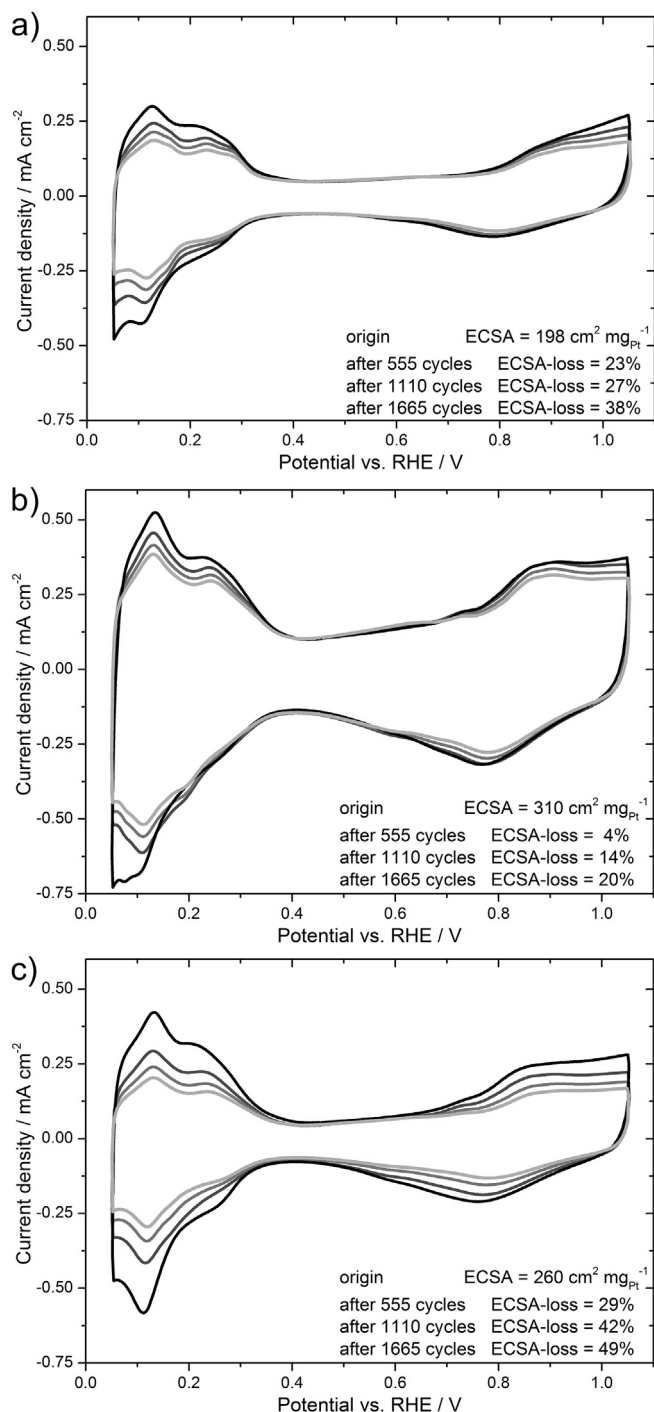
Fig. 5. Cyclic voltammograms of the untreated Pt–Co/C catalyst (a), the leached and heat treated Pt–Co/C catalyst (b) and the Pt/C catalyst (c) recorded at a scan rate of 50 mV s⁻¹ in nitrogen saturated 0.1 M HClO₄ electrolyte. The gradual degradation of the catalysts during AST cycling is given after 555, 1110 and 1665 cycles in form of the loss of ECSA.

Fig. 6. Polarization curves and power densities of the leached and heat treated Pt–Co/C based HT-PEM MEA before and after 600 h long term operation and the commercial HT-PEM MEA under constant load at 160 °C, fueled with hydrogen (a) and synthetic reformate (b) at the anode and air at the cathode.

resistances were at a constant value of 2.4 mΩ for the leached and heat treated Pt–Co/C based HT-PEM MEA and 1.7 mΩ for the commercial one, respectively. Both values indicate a good distribution of H₃PO₄ electrolyte within the catalyst layer of the cathode electrode. By comparison, both MEAs showed an equal
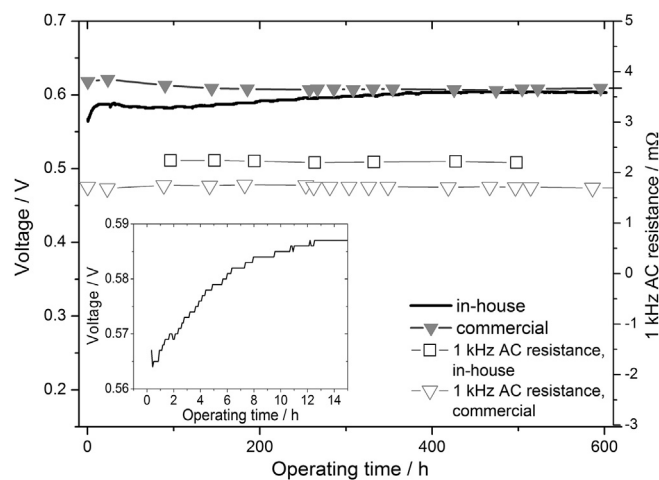
Fig. 7. Comparison of cell voltages and the corresponding 1 kHz AC resistances of the leached and heat treated Pt–Co/C based HT-PEM MEA and a commercial HT-PEM MEA during durability testing at 160 °C. The insert shows the first 14 h of the long term operation of the in-house prepared MEA.

under steady state conditions at 160 °C was 0 μV h⁻¹. Especially during the first 14 h of the long term operation a very steep increase in cell voltage was observed, followed by a constant increase up to 500 h runtime. After that, the cell voltage stabilized at 604 mV. In contrast, the commercially obtained HT-PEM MEA from elcomax GmbH showed a better performance at the beginning of the durability test, but lost cell voltage continually over the first 400 h of operation, which stabilized at 608 mV afterwards. The 1 kHz AC

performance during 600 h of operation under constant load, although the commercial HT-PEM MEA had a much higher Pt loading at the cathode.

3.3.3. Electrochemical impedance spectroscopy

EIS is a commonly applied tool in electrochemistry to investigate corrosion processes and to quantify losses occurring in electrochemical devices, such as batteries. In fuel cell research it is a reliable method, providing information on catalyst and membrane materials [46]. In general, the information on the catalyst and membrane materials derives either from a process model based on physicochemical relations, kinetics, mechanisms and consequently analytic equations or from a measurement model by means of equivalent circuit (EC) analogs. Both evaluation approaches offer advantages, but have insufficiencies as well. For example a good numerical complex nonlinear least square fit of a measurement model to experimental data does not necessarily mean the correct EC is applied. On the other hand a process model approach is often too complex to be applied on multipart systems like fuel cells. *Rezaei Niya* et al. gives a very concise comparison of these two approaches with respect to fuel cell applications [47] and *Macdonald* makes a very detailed distinction between models and analogs [48]. Due to the increasing complexity of process models with the increasing number of components in a fuel cell a measurement model based analysis is the more straight-forward approach for our HT-PEMFC investigation. Although the physical meaning of the applied EC elements may be under discussion at least correlations can be drawn between the described equivalent circuit and the analysis as follows.

Herein, EC analysis was used to simulate the entire frequency range of the given impedance spectra (e.g. Fig. 8). Therefore, electric components, such as resistors and capacitors, were used for the simulation and fitting process. The applied EC (Fig. 9) is based on the modified Randles cell equivalent circuit suggested by *Zhang* et al. [49] and its further modification as described in Ref. [50].

In Fig. 8 the recorded EIS spectra of the leached and heat treated Pt−Co/C based MEA are presented in form of their Nyquist plots. The measurement at the beginning of the long term operation shows three depressed semicircles, while after 600 h of operation a fourth arising semicircle may be observed additionally. Both impedance spectra show the same frequency dependence and are interpreted as follows.

The beginning semicircle which is observed in the very high frequency area may not be attributed to an anode charge transfer reaction since the characteristic frequency (23208 Hz) is too high to be formed by a chemical reaction. The origin of this rc element is due to contact resistance between the flowplates and the MEA while the capacitance is attributed to small amounts of H_3PO_4 at the interface between the two layers. Other explanations for such a behavior refer these potential independent high frequency
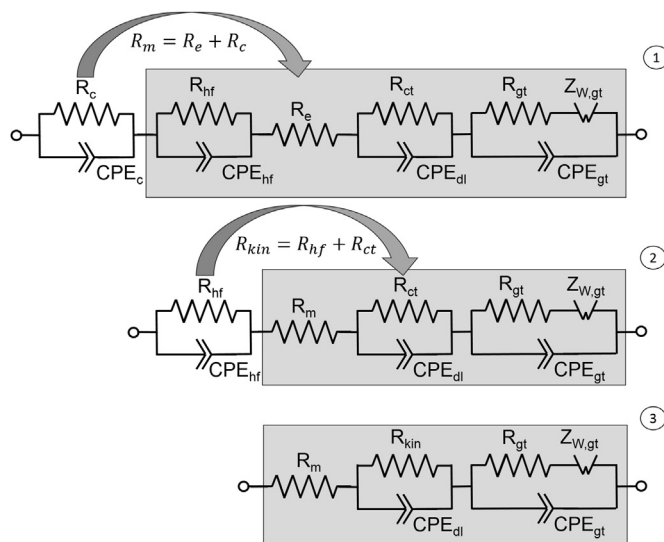

Fig. 9. Equivalent circuit which was applied for fitting procedure (1) and simplification steps (2) and (3).

semicircles to the distribution of resistance effects within the electrolyte in the catalysts layer [51,52]. This phenomenon leads to the fact that the high frequency intercept, which is commonly ascribed to the electrolyte resistance (R_e), is not seen directly within the observed frequency range. Therefore, the membrane resistance is obtained by calculating the sum of these distributed ohmic contact resistances (R_c) and the electrolyte resistance (R_e) and is in accordance with [50,53] denoted by membrane resistance (R_m).

In the mid frequency area at least one depressed semicircle is observed which is attributed mainly to the ORR charge transfer reaction. The corresponding anode impedance semicircle or anode loop is masked by the more significant ORR semicircle. Especially at the beginning of the long term operation the characteristic frequencies are too close together to be seen as separate semicircles. After 600 h of operation the characteristic frequencies have separated leading to two semicircles in the Nyquist plot and the anode reaction semicircle is observed. Since the origin of this loop is still under discussion the corresponding equivalent circuit element is better denoted by high frequency loop ($R_{hf}\|CPE_{hf}$) than by anode loop [54].

In the low frequency area mass transport limitations are observed in both spectra, but are more significant after 600 h of operation. Additionally, the fluctuations in the low frequency arc indicate a slight flooding event. According to this interpretation the equivalent circuit shown in Fig. 9 was applied for our fitting procedure and simplified for the discussion.

The for the fitting procedure applied formulas as well as the obtained parameters are shown in Table 4, where the kinetic
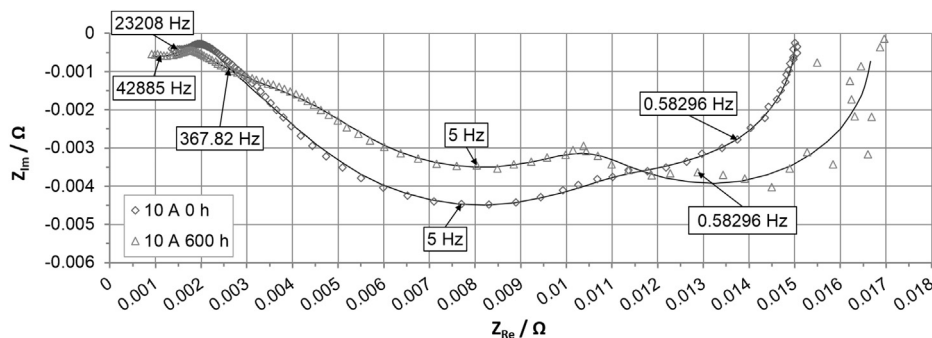

Fig. 8. Nyquist plots of the EIS measurements of the leached and heat treated Pt−Co/C based HT-PEM MEA at BoL and after 600 h of operation.

resistance R_{kin} is the sum of the charge transfer and high frequency resistances ($R_{ct} + R_{hf}$). The membrane resistance R_m is, as described above, the sum of the ohmic contact resistances (R_c) and the electrolyte resistance (R_e). R_{gt} specifies the resistance occurring by the transport of the reactant gases through the porous layer of the GDE. The overall Warburg impedance Z_W is calculated from the Warburg diffusion interpretation parameter T_W, the finite length Warburg resistance R_W and the Warburg exponent P_W. The second column of Table 4 specifies the different coefficients T_{ct}, T_{hf}, T_c and T_{gt} and their corresponding exponents P_{ct}, P_{hf}, P_c and P_{gt} of the constant phase elements (CPEs) given in Fig. 9. All of these parameters exhibit changes during the long term operation experiment. After the first step of simplification it is seen that the membrane resistance R_m ($= R_c + R_e$, see Table 4) has decreased starting from 1.95 mΩ to 1.53 mΩ which is slightly lower than the obtained 1 kHz AC resistance (Fig. 7) recorded throughout the long term experiment. This decrease indicates an improved electrolyte distribution within the active layer, which leads to a decrease of R_c and R_m, respectively. Furthermore, it indicates that the main part of the membrane resistance rather originates from an insufficient electrolyte distribution in the active layer than from the electrolyte resistance itself.

The decrease in the diameter of the mid frequency semicircle ($R_{kin} = R_{ct} + R_{hf}$) is also due to the improved electrolyte distribution within the catalysts layer. During the operation the exponent (P_{dl}) of the constant phase element ascribed to the double layer (CPE_{dl}) decreased as well, which generally indicates a broader distribution of time constants and a better distribution of H_3PO_4. Both tendencies, the decreased R_{kin} as well as the decreased P_{dl}, indicate an increased active catalyst surface area due to an improved H_3PO_4 distribution. But nevertheless, the fractional increase of the obtained ECSA by CV analysis (see Fig. 10) goes beyond the fractional increase of the kinetic conductance (Table 5). This difference may be explained by the surface roughening effect of the catalysts particles, which increases the accessible inner surface of the catalysts particles and consequently the obtained ECSA.

In Fig. 10 the cyclic voltammograms of the leached and heat treated Pt—Co/C based HT-PEM MEA before and after the durability test are shown. During operation the ECSA of the cathode catalysts layer increased slightly from 104 to 113 cm² mg$_{Pt}^{-1}$. This enlargement of the active surface area can be attributed either to the redistribution of the H_3PO_4 electrolyte in the doped catalysts layer, resulting in an improved membrane resistance ($R_m = R_e + R_c$) as well as kinetic conductance ($S_{kin} = 1/R_{kin}$), as observed in EIS measurements, or to an additional removal of impurities and inactive Co sites at the surface of the GDE.

According to the obtained parameters (Table 4) the diameter of the low frequency semicircle which is observed more clearly after
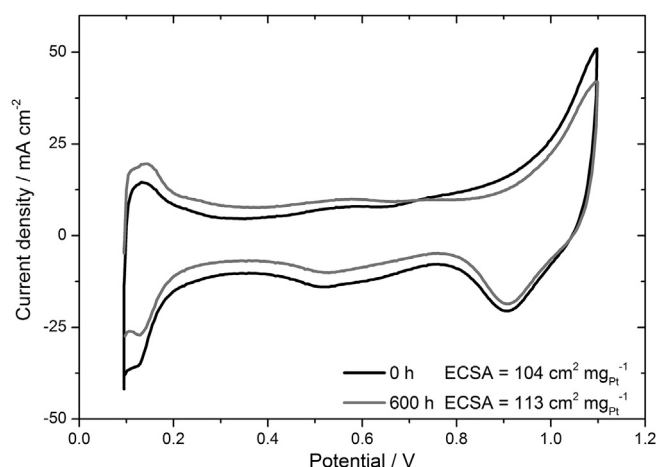

Fig. 10. Cyclic voltammograms of the cathode layer of the leached and heat treated Pt—Co/C based HT-PEM MEA before and after long term operation test, recorded at a scan rate of 50 mV s^{-1}. The anode (fed with dry hydrogen) was used as pseudo-reference electrode. The cathode was supplied with humidified nitrogen.

600 h of operation under constant load is increased. This may also be attributed to an increased wetting of the active layer and consequently longer diffusion pathways when thinking of a flooded agglomerate model [55]. The fluctuations in the low frequency arc also indicate a slight flooding of the active layer although the polarization curve does not indicate such an issue.

4. Conclusion and outlook

In this paper we have presented roll-to-roll processed Pt-M/C catalysts as part of an economic and flexible large scale MEA manufacturing for application as cathode catalysts in PBI-based HT-PEM fuel cells. During production it has been paid attention to keep the synthesis of the catalysts as simple as possible. To obtain a higher Pt utilization the continuous deposition of the catalysts was achieved directly in the optimized porous layer of the gas diffusion electrode. In contrast to conventional casting of catalyst loaded HSAC onto the GDL, the loss of Pt during production is reduced by the presented process, rendering it more economical. Furthermore, Pt enclosures in carbon aggregates are eliminated and due to the absence of batch processes, such as filtering, centrifugation, multiple washing, drying and annealing in tube furnaces, the herein presented continuous MEA fabrication is much more time and cost saving.

After post preparation treatment, such as acid-leaching and annealing, the developed Pt—Co catalysts exhibit good catalytic properties and enhanced stability in ex-situ tests. In comparison to

Table 4
Parameters obtained by the EC fitting procedure (*: fixed parameters).

		0 h	600 h		0 h	600 h
$^0R_{kin}$	R_{ct}/Ω	5.01E-03	4.99E-03	$^2T_{dl}$/A V^{-1} dim[(jω)$^{-P}$]	1.17E+01	7.91E+00
	R_{hf}/Ω	4.81E-03	4.61E-03	$^2T_{hf}$/A V^{-1} dim[(jω)$^{-P}$]	5.10E+00	6.29E+00
$^0R_{m}$	R_{c}/Ω	1.48E-03	1.21E-03	$^2T_{c}$/A V^{-1} dim[(jω)$^{-P}$]	1.00E-02	1.00E-02
	R_{e}/Ω	4.70E-04	3.18E-04	$^2T_{gt}$/A V^{-1} dim[(jω)$^{-P}$]	50.4E+00	57.4E+00
R_{gt}	R_{gt}/Ω	3.08E-05	1.17E-03	$^2P_{dl}$	6.43E-01	5.59E-01
^1Z_W	T_W	3.77E-04	3.77E-04	$^2P_{hf}$	1.09E+00	1.02E+00
	R_{W}/Ω	3.27E-03	4.41E-03	$^2P_{c}$	8.58E-01	9.00E-01
	$^*P_W$	**0.5**	**0.5**	$^2P_{gt}$	1.10E+00	1.10E+00

$^0R_{kin} = R_{ct} + R_{hf}$

$^1Z_W = R_W \dfrac{\tanh[(j\omega T_w)^{P_w}]}{(j\omega T_w)^{P_w}}$

$^2Z_{CPE} = \dfrac{1}{T_x(j\omega)^{P_x}}$

Applied formulas
j = square root of −1; ω = angular frequency/rad s^{-1}

Table 5
The ECSA increase vs. the increase of the kinetic conductance ($S_{kin} = 1/R_{kin}$).

	ECSA/cm^2 mg$_{Pt}^{-1}$	R_{Kin}/Ω	S_{Kin}/Ω^{-1}
0 h	104	9.82E-03	102
600 h	113	9.60E-03	104
Ratio	1.09		1.02

reported Pt$_3$Co catalysts, which have been prepared by laborious and expensive production processes, our Pt—Co catalysts lack in high specific and mass activity toward oxygen reduction reaction under ex-situ conditions. Though, under in-situ conditions our catalysts perform equally to commercially available Pt catalysts or even outperform them.

The begin-of-lifetime polarization curves, which were obtained directly after hot-pressing of the leached and heat treated Pt—Co/C based HT-PEM MEA, show a poor performance. Within the first 14 h of operation at constant load a steep increase of the cell performance was observed. We ascribe this voltage gain to the redistribution of the electrolyte within the cathode catalyst layer after hot-pressing and to a further cleaning of the catalysts surface. EIS measurements, recorded in synthetic reformate, and fitting of the data thereof confirm our assumption. After the steep increase the cell voltage stabilized at 604 mV for the remaining test period. A comparison of the polarization curves taken before and after the long term HT-PEM test for 600 h showed a significant increase of cell performance and OCV.

By using our newly developed catalyst deposition system we achieved a reduction of the platinum loading of HT-PEM MEA cathodes without loss of performance.

Currently, a fuel cell stack test including long term operation with natural gas reformate is under progress. With these results we will gain further insight into the durability of our Pt—Co/C catalyst system and its feasibility for HT-PEM fuel cell systems.

Acknowledgments

References

[1] I.E.L. Stephens, A.S. Bondarenko, U. Grønbjerg, J. Rossmeisl, I. Chorkendorff, Energy Environ. Sci. 5 (2012) 6744.
[2] K.C. Neyerlin, W. Gu, J. Jorne, H.A. Gasteiger, J. Electrochem. Soc. 154 (2007) B631.
[3] H.A. Gasteiger, S.S. Kocha, B. Sompalli, F.T. Wagner, Appl. Catal. B Environ. 56 (2005) 9.
[4] J.K. Nørskov, J. Rossmeisl, A. Logadottir, L. Lindqvist, J.R. Kitchin, T. Bligaard, H. Jónsson, J. Phys. Chem. B 108 (2004) 17886.
[5] S.-K. Kim, K.-H. Kim, J.O. Park, K. Kim, T. Ko, S.-W. Choi, C. Pak, H. Chang, J.-C. Lee, J. Power Sources 226 (2013) 346.
[6] R. Bashyam, P. Zelenay, Nature 443 (2006) 63.
[7] M.S. Thorum, J. Yadav, A.A. Gewirth, Angew. Chem. Int. Ed. Engl. 48 (2009) 165.
[8] G. Wu, K.L. More, C.M. Johnston, P. Zelenay, Science 332 (2011) 443.
[9] F. Calle-Vallejo, J.I. Martínez, J. Rossmeisl, Phys. Chem. Chem. Phys. 13 (2011) 15639.
[10] M. Lefèvre, E. Proietti, F. Jaouen, J.-P. Dodelet, Science 324 (2009) 71.
[11] Y. Gorlin, T.F. Jaramillo, J. Am. Chem. Soc. 132 (2010) 13612.
[12] J. Suntivich, H.A. Gasteiger, N. Yabuuchi, Y. Shao-Horn, J. Electrochem. Soc. 157 (2010) B1263.
[13] M. Escudero-Escribano, A. Verdaguer-Casadevall, P. Malacrida, U. Grønbjerg, B.P. Knudsen, A.K. Jepsen, J. Rossmeisl, I.E.L. Stephens, I. Chorkendorff, J. Am. Chem. Soc. 134 (2012) 16476.
[14] V.R. Stamenkovic, B.S. Mun, M. Arenz, K.J.J. Mayrhofer, C.A. Lucas, G. Wang, P.N. Ross, N.M. Markovic, Nat. Mater. 6 (2007) 241.
[15] J.R. Kitchin, J.K. Nørskov, M.A. Barteau, J.G. Chen, J. Chem. Phys. 120 (2004) 10240.
[16] V.R. Stamenkovic, B. Fowler, B.S. Mun, G. Wang, P.N. Ross, C.A. Lucas, N.M. Markovic, Science 315 (2007) 493.
[17] T. Toda, H. Igarashi, H. Uchida, M. Watanabe, J. Electrochem. Soc. 146 (1999) 3750.
[18] X. Liu, G. Fu, Y. Chen, Y. Tang, P. She, T. Lu, Chemistry 20 (2014) 585.
[19] G. Fu, K. Wu, J. Lin, Y. Tang, Y. Chen, Y. Zhou, T. Lu, J. Phys. Chem. C 117 (2013) 9826.
[20] E. Antolini, T. Lopes, E.R. Gonzalez, J. Alloys Compd. 461 (2008) 253.
[21] B.C. Beard, P.N. Ross, J. Electrochem. Soc. 137 (1990) 3368.
[22] V.R. Stamenkovic, T.J. Schmidt, P.N. Ross, N.M. Markovic, J. Phys. Chem. B 106 (2002) 11970.
[23] N.M. Markovic, T.J. Schmidt, V.R. Stamenkovic, P.N. Ross, Fuel Cells 1 (2001) 105.
[24] J.R.C. Salgado, E. Antolini, E.R. Gonzalez, J. Power Sources 141 (2005) 13.
[25] J.R.C. Salgado, E. Antolini, E.R. Gonzalez, J. Power Sources 138 (2004) 56.
[26] T. Lopes, E. Antolini, F. Colmati, E.R. Gonzalez, J. Power Sources 164 (2007) 111.
[27] E. Antolini, J.R.C. Salgado, E.R. Gonzalez, J. Electroanal. Chem. 580 (2005) 145.
[28] I. Spanos, J.J.K. Kirkensgaard, K. Mortensen, M. Arenz, J. Power Sources 245 (2014) 908.
[29] K. Jayasayee, J.A.R. Van Veen, T.G. Manivasagam, S. Celebi, E.J.M. Hensen, F.A. de Bruijn, Appl. Catal. B Environ. 111—112 (2012) 515.
[30] K.J.J. Mayrhofer, K. Hartl, V. Juhart, M. Arenz, J. Am. Chem. Soc. 131 (2009) 16348.
[31] S.C. Zignani, E. Antolini, E.R. Gonzalez, J. Power Sources 182 (2008) 83.
[32] E. Antolini, J.R.C. Salgado, E.R. Gonzalez, J. Power Sources 160 (2006) 957.
[33] V.R. Stamenkovic, B.S. Mun, K.J.J. Mayrhofer, P.N. Ross, N.M. Markovic, J. Am. Chem. Soc. 128 (2006) 8813.
[34] C. Wang, M. Chi, D. Li, D. Strmcnik, D. van der Vliet, G. Wang, V. Komanicky, K.-C. Chang, A.P. Paulikas, D. Tripkovic, J. Pearson, K.L. More, N.M. Markovic, V.R. Stamenkovic, J. Am. Chem. Soc. 133 (2011) 14396.
[35] C. Wang, D. van der Vliet, K.L. More, N.J. Zaluzec, S. Peng, S. Sun, H. Daimon, G. Wang, J. Greeley, J. Pearson, A.P. Paulikas, G. Karapetrov, D. Strmcnik, N.M. Markovic, V.R. Stamenkovic, Nano Lett. 11 (2011) 919.
[36] H.E. Swanson, E. Tatge, Natl. Bur. Stand. Circ. 539 (1953) 1.
[37] E.A. Owen, D. Madoc Jones, Proc. Phys. Soc. Sect. B 67 (1954) 456.
[38] A.S. Darling, Platin. Met. Rev. (1963) 96.
[39] P. Scherrer, Nachr. Ges. Wiss. Göttingen 26 (1918) 98.
[40] Y. Garsany, O.A. Baturina, K.E. Swider-Lyons, S.S. Kocha, Anal. Chem. 82 (2010) 6321.
[41] K.J.J. Mayrhofer, D. Strmcnik, B.B. Blizanac, V.R. Stamenkovic, M. Arenz, N.M. Markovic, Electrochim. Acta 53 (2008) 3181.
[42] R.W.G. Wyckoff, The Structure of Crystals, second ed., vol. 1, Interscience Publishers, New York, 1963.
[43] E.I. Santiago, L.C. Varanda, H.M. Villullas, J. Phys. Chem. C 111 (2007) 3146.
[44] P. Strasser, S. Koh, T. Anniyev, J. Greeley, K. More, C. Yu, Z. Liu, S. Kaya, D. Nordlund, H. Ogasawara, M.F. Toney, A. Nilsson, Nat. Chem. 2 (2010) 454.
[45] L. Xiong, A. Manthiram, Electrochim. Acta 50 (2005) 2323.
[46] M.E. Orazem, B. Tribollet, Electrochemical Impedance Spectroscopy, John Wiley & Sons, Inc., Hoboken, New Jersey, 2008.
[47] S.M. Rezaei Niya, M. Hoorfar, J. Power Sources 240 (2013) 281.
[48] D.D. Macdonald, Electrochim. Acta 51 (2006) 1376.
[49] J. Zhang, Y. Tang, C. Song, J. Zhang, J. Power Sources 172 (2007) 163.
[50] J. Jespersen, E. Schaltz, S. Kær, J. Power Sources 191 (2009) 289.
[51] X. Yuan, H. Wang, J.C. Sun, J. Zhang, Int. J. Hydrogen Energy 32 (2007) 4365.
[52] T.J.P. Freire, E.R. Gonzalez, J. Electroanal. Chem. 503 (2001) 57.
[53] W.H. Zhu, R.U. Payne, B.J. Tatarchuk, J. Power Sources 168 (2007) 211.
[54] X. Yuan, J.C. Sun, M. Blanco, H. Wang, J. Zhang, D.P. Wilkinson, J. Power Sources 161 (2006) 920.
[55] S. Kamarajugadda, S. Mazumder, J. Power Sources 208 (2012) 328.